THE BANANA PROJECT. III. SPIN-ORBIT ALIGNMENT IN THE LONG-PERIOD ECLIPSING BINARY NY CEPHEI[*]

Simon Albrecht[1], Joshua N. Winn[1], Joshua A. Carter[1],
Ignas A. G. Snellen[2], Ernst J. W. de Mooij[2]

[1]Department of Physics, and Kavli Institute for Astrophysics and Space Research,
Massachusetts Institute of Technology, Cambridge, MA 02139, USA and
[2]Leiden Observatory, Leiden University, Postbus 9513, 2300 RA Leiden, The Netherlands

Draft version November 8, 2010

ABSTRACT

Binaries are not always neatly aligned. Previous observations of the DI Her system showed that the spin axes of both stars are highly inclined with respect to one another and the orbital axis. Here we report on a measurement of the spin-axis orientation of the primary star of the NY Cep system, which is similar to DI Her in many respects: it features two young early-type stars ($\sim$ 6Myr, B0.5V+B2V), in an eccentric and relatively long-period orbit ($e = 0.48$, $P = 15\overset{\text{d}}{.}3$). The sky projections of the rotation vector and the spin vector are well-aligned ($\beta_{\rm p} = 2 \pm 4°$), in strong contrast to DI Her. Although no convincing explanation has yet been given for the misalignment of DI Her, our results show that the phenomenon is not universal, and that a successful theory will need to account for the different outcome in the case of NY Cep.

Subject headings: techniques: spectroscopic—stars: kinematics and dynamics—stars: early-type—stars: rotation—stars: formation—binaries: eclipsing—stars: individual (NY Cep)

1. INTRODUCTION

We are conducting measurements of the relative orientations of the rotational and orbital axes in close binary star systems. Our name for this undertaking is the Banana project, an acronym chosen to remind us that binaries are not always neatly aligned. This paper reports our results for the NY Cephei system, the third system we have studied, the first two having been V1143 Cygni (Albrecht et al. 2007) and DI Herculis (Albrecht et al. 2009). Those two earlier works were written before our project was enlarged and named, and are retrospectively included in this series as Papers I and II. The goal of the Banana project is to enlarge the number of detached binary systems for which the relative orientation of the spin axes is known, in order to shed light on the formation and evolution of binaries and perhaps also of planets.

1.1. *Motivation*

Close binaries and star-planet systems might be expected to have well-aligned orbital and spin angular momenta, since all of the components trace back to the same portion of a molecular cloud. However, good alignment is not guaranteed. If a cloud is highly elongated, with its long axis tilted with respect to its rotation axis, then the cloud may give birth to binary stars with a strong spin-orbit misalignment (Bonnell et al. 1992). Alternatively, disks around young stars might become warped during the last stage of accretion. This warp could torque the orbit by a large angle while maintaining the orientation of the spins (Tremaine 1991). More generally, star formation may be a chaotic process, with accretion from different directions at different times (Bate et al. 2010),

albrecht@space.mit.edu

* Based on observations made with *Sophie*, a high-resolution échelle spectrograph on the 1.93-m telescope of the Observatoire de Haute-Provence.

and perhaps we should not expect the angular momenta of the star and the disk to be as well aligned as they apparently were in the Solar system.

There are also processes that could alter the stellar and orbital spin directions after their formation. A third body orbiting a close pair on a highly inclined orbit can introduce large oscillations in the orbital inclination and eccentricity of the close pair (Kozai 1962). Tidal dissipation during the high-eccentricity phases can cause the system to free itself of these "Kozai oscillations" and become stuck in a high-obliquity state (Fabrycky & Tremaine 2007). However, if dissipation is sufficiently strong then the system will evolve into the double-synchronous state, characterized by spin-orbit alignment (e.g. Hut 1981). Therefore, whether a close binary or a star-planet system is well-aligned or misaligned depends on its particular history of formation and evolution. Even though this issue is important for a complete understanding of star formation, there has been very little observational input.

Another motivation comes from exoplanetary science. Recently it was revealed that many of the close-in giant planets ("hot Jupiters") have orbits that are strongly misaligned with the rotation axes of their parent stars (see, e.g., Hébrard et al. 2008; Winn et al. 2009; Narita et al. 2009; Triaud et al. 2010). The high obliquities are especially common among stars with higher masses and effective temperatures (Winn et al. 2010; Schlaufman 2010). The results of such studies are commonly interpreted as constraints on theories of the "migration" processes that presumably brought the planets inward from their more distant birthplaces. However, some theories invoke processes that produce large stellar obliquities for reasons having nothing to do with the planets, such as chaotic accretion (Bate et al. 2010), and magnetic interactions with the inner edge of the accretion disk (Lai et al. 2010). Although those theories have not been fully

TABLE 1
MEASUREMENTS OF SPIN ORBIT ANGLES IN ECLIPSING BINARIES

System	Spectral Type	Period [d]	$r_{\rm p}$	Eccentricity (e)	$\beta[°]$	reference
β Lyr	Be+B6-8II	12.9	0.52	<0.01	aligned?	1,2
V1010 Oph	A7IV-V+?	0.66	0.4511±0.011	≡ 0	aligned?	3,4
W Umi	A3V+G9IV	1.7	0.363±0.001	≡ 0	aligned?	5
δ Lib	A0V+K0IV	2.33	0.30±0.06	≡ 0	aligned?	6,7
V505 Sgr	A2V+GIV	1.2	0.288±0.001	≡ 0	aligned?	8,9
AI Dra	A0V+F9.5V	1.2	0.284±0.004	≡ 0	aligned?	8,10
X Tri	A3V+G3IV	0.97	0.272±0.003	≡ 0	aligned?	5
RZ Cas	A3V+KIV	1.20	0.233±0.001	≡ 0	aligned?	5
U Sge	B8.5V+G3III	3.38	0.219±0.002	0.04	aligned?	5
WW Cyg	B8V+G4III	3.32	0.215±0.002	≡ 0	aligned?	5
Y Leo	A3V+K3IV	1.69	0.213±0.001	≡ 0	aligned?	5
RX Hya	A8+K0IV	2.28	0.211±0.013	≡ 0	aligned?	5
Algol	B8+K2IV	2.87	0.206±0.003	≡ 0	aligned?	11,12,13
RW Gem	B5-B6V+F0III	2.87	0.198±0.002	≡ 0	aligned?	5
Y Psc	A3V+K2IV	3.77	0.193±0.001	0.12	aligned?	5
TV Cas	A2V+G1IV	1.81	0.188±0.15	≡ 0	aligned?	5
ST Per	A3V+KIV	2.65	0.184±0.004	≡ 0	aligned?	5
U Cep	B7V+G8III	2.49	0.177±0.009	≡ 0	aligned?	5
TX Uma	B8V+F7-F8III	3.06	0.164±0.002	≡ 0	aligned?	5
W Del	A0-B9.5V+K0IV	4.81	0.151±0.004	0.20	aligned?	5
AA Dor	sdOB+?	0.26	0.14±0.01	≡ 0	aligned?	14
DE Dra	B0V+B2V	5.3	0.14	0.018±0.011	misaligned?	15
SW Syg	A2V+K1IV	4.57	0.138±0.002	0.30	aligned?	5
RY Per	B4V+F0III	6.86	0.137±0.003	0.21	aligned?	5
RZ Sct	B2II+A0II-III	15.19	0.136±0.007	≡ 0	aligned?	5
AQ Peg	A2V+K1IV	5.55	0.123±0.002	0.24	aligned?	5
RY Gem	A2V+K0III-K1IV	9.30	0.097±0.014	0.16	aligned?	5
NY Cep	B0V+B2V	15.3	0.086±0.015	0.445±0.004	$\beta_{\rm p} = 2° \pm 4°$	16,17
DI Her	B4V+B5V	10.55	0.0621±0.001	0.489±0.003	$\beta_{\rm p} = 72° \pm 4°, \beta_{\rm s} = -84° \pm 8°$	18,19
V1143 Cyg	F5V+F5V	7.64	0.059±0.001	0.5378±0.0003	$\beta_{\rm p} = 0°3 \pm 1°5, \beta_{\rm s} = -1°2 \pm 1°6$	20,21

NOTE. — In column 4, $r_{\rm p}$ denotes the radius of the primary star divided by the length of the orbital semimajor axis. For DE Dra and β Lyr no uncertainties in the primary radii are given in the references. In column 5, the entry "≡ 0" indicates that the eccentricity was assumed to be zero by the authors. In column 6, $\beta_{\rm p}$ and $\beta_{\rm s}$ denote angles between the projections of stellar and orbital spin axes for the primary and secondary, respectively, using the coordinate system of Hosokawa (1953).

REFERENCES. — (1) Rossiter (1924); (2) Harmanec (2002); (3) Worek et al. (1988) (4) Corcoran et al. (1991); (5) Twigg (1979); (6) Bakış et al. (2006); (7) Worek (1985); (8) Worek (1996); (9) Lázaro et al. (2006); (10) Lázaro et al. (2004); (11) McLaughlin (1924); (12) Struve & Elvey (1931); (13) Soderhjelm (1980); (14) Rucinski (2009); (15) Hube & Couch (1982); (16) Holmgren et al. (1990); (17) This study; (18) Popper (1982); (19) Albrecht et al. (2009); (20) Andersen et al. (1987); (21) Albrecht et al. (2007)

developed, it would seem that the mechanisms they propose should also operate in the case of binary stars, and therefore the theories might be tested by measuring the obliquities of binary stars.

For example if interactions with a distant companion are important for close double stars, then this should also be true for star-planet systems. Other effects like tidal realignment do depend on the mass and mass ratio of the close pair. For a direct comparison with the exoplanet hosts, one would want to survey main sequence F and G binaries, while (as we will describe) most of the existing data, including the data presented in this paper, is for earlier type stars. We hope to rectify this situation with future observations.

1.2. *Measuring stellar obliquities*

Measuring the orientations of stellar spin axes is not straightforward. Telescopes cannot usually resolve stellar disks, causing the information on spatial orientation to be lost. An optical interferometer, in combination with a high resolution spectrograph, might allow for spatial resolution of rotationally-broadened stellar absorp-

tion lines (Petrov 1989; Chelli & Petrov 1995), but so far such measurements are possible for only the very nearest and brightest systems (Le Bouquin et al. 2009).

One would be able to determine the inclinations of the spin axes with respect to the sky plane, based on empirical estimates of the projected stellar rotation speed ($v \sin i$), the stellar radius ($R_\star$), and the stellar rotation period ($P_{\rm rot}$), using the equation

$$ i = \sin^{-1}\left[\frac{v \sin i}{(2\pi R_\star / P_{\rm rot})}\right]. \tag{1} $$

Many investigators have pursued this path and found it to be blocked, for reasons described clearly by Soderblom (1985). Namely, the quantities $v \sin i$, $R_\star$, and $P_{\rm rot}$ are difficult to measure with high enough accuracy, and the flattening of the sine function near 90° prevents the method from discriminating even modest inclinations from edge-on inclinations. Despite these difficulties, Glebocki & Stawikowski (1997) used this method to argue that active binaries that are observed to be asynchronously rotating have misaligned spin axes.

Given a large sample of $v \sin i$ measurements of stars

TABLE 2
GENERAL DATA ON NY CEPHEI

HIP	113461	
HD	217312	
R.A.$_{\rm J2000}$	$22^{\rm h}58^{\rm m}40^{\rm s}$	‡
Dec.$_{\rm J2000}$	$63°04'38''$	‡
V$_{\rm max}$	7.5 mag	‡
Sp. Type	B0.5V+ B2V	⋆
Period	$15^{\rm d}.27$	†
Eccentricity	0.48(2)	⋆
Inclination	78(1)°	⋆
R$_{\rm p}$	$6.8(7)R_\odot$	⋆
R$_{\rm s}$	$5.4(5)R_\odot$	⋆
M$_{\rm p}$	$13(1)M_\odot$	⋆
M$_{\rm s}$	$9(1)M_\odot$	⋆
L$_{\rm s}$/L$_{\rm p}$	0.37(6)	⋆

‡Data from ESA (1997)
†Data from Ahn (1992)
⋆Data from Holmgren et al. (1990)

NOTE. — R$_{\rm p}$ denotes the radius of the primary component and R$_{\rm s}$ the radius of the secondary component. L$_{\rm p}$/L$_{\rm s}$ denotes the luminosity ratio between the primary and secondary.
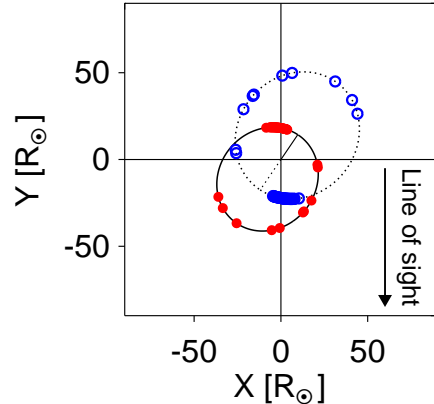

FIG. 1.— **Pole-on view of the orbit of NY Cep.** The solid and dashed ellipses indicate the orbits of the primary and secondary stars, respectively. The filled (red) circles indicate the positions of primary star and the open (blue) circles indicate the position of the secondary star during times of observations. The lines connecting the orbits with the center of gravity indicate the position of periastron. We observe the system from the x origin and a negative y value.

that have a known distribution of rotation speeds, or that are presumed to have similar rotation speeds (e.g., main-sequence stars of a given mass and age), it is possible to test for departures from an isotropic distribution of spin directions. Using this idea, Guthrie (1985) and Abt (2001) searched for, and did not find, a tendency for stars to be preferentially aligned with the Galactic plane. When the orbital orientation is also known, as is the case for visual binaries or eclipsing binaries, then such tests give information about spin-orbit alignment. Such studies are worthwhile but they are hampered by the nonlinearity of the sine function (as mentioned above) as well as uncertainty in the underlying distribution of rotational speeds, and the heterogeneity in the techniques for measuring $v \sin i$. This method has been used in various guises by Weis (1974), Hale (1994), and Howe & Clarke (2009), among others. Recently, Schlaufman (2010) used this method on stars with transiting planets, finding evidence that more massive stars have high obliquities.

Indirect evidence on the orientation of young stars comes from the orientation of their disks – assuming star-disk alignment. The projected rotation angle of the disk can be traced by the linear polarization vector of the star light reflected from the dust grains in disks (Monin et al. 1998). These authors and others (e.g. Donar et al. 1999; Wolf et al. 2001; Jensen et al. 2004; Monin et al. 2006) find that in most binary systems the disks around the individual stars are aligned with each other. However they also mention exceptions to this rule. One of these exceptions is the hierarchical triple system T Tauri, for which Skemer et al. (2008) and Ratzka et al. (2009) found that the disk around the northern component, the original T Tauri system, is viewed face on, while the disk around one of the southern components (T Tau Sa), separated by $\gtrsim 100$ AU from T Tau N, is viewed edge-on. Thus this system has misaligned circumstellar disks.

The method that provides the most accurate information for individual systems takes advantage of eclipses.

During an eclipse of one star by another star or a planet, part of the rotating stellar surface is hidden, causing a weakening of the corresponding velocity component of the stellar absorption lines. Modeling of this spectral distortion reveals the relative orientation of the spin and orbital axes on the sky: the *projected obliquity*. This "rotation anomaly" was first predicted by Holt (1893). A claim of its detection in the δ Librae system was made by Schlesinger (1910), but more definitive measurements were achieved by Rossiter (1924) and McLaughlin (1924) for the β Lyrae and Algol systems, respectively. The phenomenon is now known as the Rossiter-McLaughlin (RM) effect. Various aspects of the theory of the effect have been worked out by Struve & Elvey (1931); Hosokawa (1953); Kopal (1959); Sato (1974); Ohta et al. (2005); Giménez (2006); Hadrava (2009), and Hirano et al. (2010). The work described in this paper, as well as in the previous papers in this series, is based on the RM effect.

1.3. *Previous observations of the RM effect*

Although it has been more than 80 years since its discovery, there are relatively few quantitative analyses of the RM effect observed in stellar binaries. It is ironic that at present, there are more such papers about exoplanetary systems than about stellar binaries. In the past, observing the RM effect was generally either avoided (as a hindrance to measuring accurate spectroscopic orbits) or used to estimate stellar rotation speeds. Almost all authors explicitly or implicitly assumed that the orbital and stellar spins were aligned.

Table 1 shows the results our literature search for analyses of the RM effect in stellar binaries. (This table also gives the results for NY Cep, the subject of this paper.) We have tried to be comprehensive, but cannot claim our list to be complete. The authors would appreciate being notified of any omissions. The systems are listed in order of decreasing $r_{\rm p}$, the radius of the primary star in units
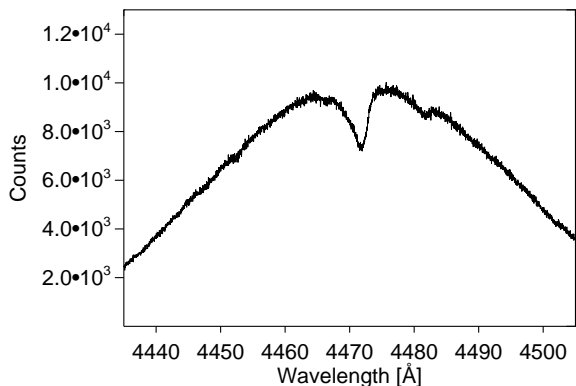
Fig. 2.— **Example spectrum of NY Cep.** Displayed is order number 11 of one spectrum of NY Cep, as delivered by the instrument software. No flat fielding, binning, or any other modifications to the data have been applied. The strong feature at 4471 Å is the He I line. Adjacent to this line, at 4481 Å, is the Mg II line.
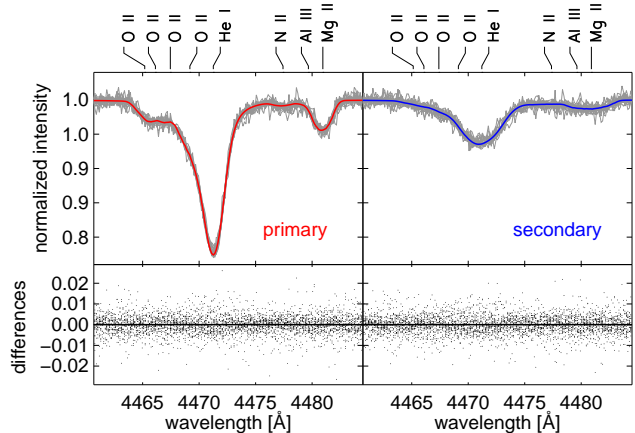

Fig. 3.— **Disentangled spectra of the two stars in the NY Cep system.** The two upper panels show spectra between 4461 Å and 4484 Å. The upper left panel is based on the sum of all the spectra obtained outside of the eclipse, after shifting into the rest frame of the primary star and after subtracting our best-fitting model of the secondary spectrum. The data are shown as gray lines, and the model as a continuous curve. The wavelengths of the lines used to construct the model spectrum are indicated above the panel. The lower left panel shows the difference between the data and the model. The right panels show the secondary spectrum, after subtracting the best-fitting model of the primary spectrum. For examples of the observed spectra with both stars present, see figures 6 and 7.

of the orbital semimajor axis, and thus the ordering is approximately a progression from closely-interacting systems to well-detached systems (although this is not true for some of the Algol systems, which have large faint secondaries). Column 6 summarizes the results for the stellar obliquities. In most cases we have written "aligned?" because the RM data appear visually to display the pattern of a well-aligned system—a redshift during the first half of the eclipse, followed by a blueshift of equal amplitude during the second half of the eclipse—with the question mark indicating that no quantitative analysis was undertaken, and hence the uncertainty is unknown. For systems with orbital inclinations very close to 90° the results are especially ambiguous because in such cases there is a strong degeneracy between the projected obliquities and rotation rates (Gaudi & Winn 2007). For DE Dra we wrote "misaligned?" because Hube & Couch (1982) found the RM effect to be asymmetric about the mideclipse time, but gave no quantitative result for the projected obliquity. The only cases where quantitative results for the projected obliquities are given are from the Banana project.

1.4. *The Banana project and NY Cep*

For our program, we have begun by concentrating on relatively young, detached systems with $r_{\rm p} < 0.15$, in order to minimize the effects of tidal interaction, and thereby study a more "primordial" distribution of obliquities. We also omit Algol-type systems, to avoid the extra complexity of the spin evolution caused by mass transfer between the stars. These criteria exclude the Algol-type systems studied by Twigg (1979) as well as all the systems listed in Table 1 except for DE Dra, V1143 Cyg, DI Her, and NY Cep. The result of misalignment in the DE Dra system by Hube & Couch (1982) is intriguing but needs to be checked. For V1143 Cygni we showed that both spin axes are well-aligned with the orbital axis [Paper I; Albrecht et al. (2007)]. In contrast, for our second target, DI Her, we measured spin axes that are drastically misaligned with the orbital axis [Paper II; Albrecht et al. (2009)]. This was the first clear

demonstration of such a strong misalignment in a close binary. It resolved the longstanding problem of the system's anomalous apsidal motion.

In this paper we focus on the NY Cephei system, whose properties are summarized in Table 2. A summary of the history of observations of this system was given by Ahn (1992). It harbors two early B type stars on an eccentric $15.^{\rm d}27$ orbit. One peculiar characteristic of this system is the lack of secondary eclipses. Inferior conjunction occurs when the stars are relatively far apart, and with an orbital inclination of $\lesssim 80°$ the sky-projected separation of the stars is too large for eclipses. The orientation of the orbit is illustrated in Figure 1.

Section 2 of this paper presents our observations and describes our model for the spectroscopic data, and our analysis procedure. The results for the orbital and stellar parameters, including the measurement of the stellar orientation are presented in section 3. The results are discussed in section 4.

2. OBSERVATIONS AND DATA REDUCTION

We observed NY Cep with *Sophie*, a high-resolution échelle spectrograph on the 1.93-m telescope of the Observatoire de Haute-Provence (Perruchot et al. 2008), employing its High Efficiency (R $\approx$ 40,000) mode. We chose an integration time of 20 min resulting in signal-to-noise ratios (SNR) between 50 and 150 per pixel at wavelengths near 4,500 Å, the spectral region used for our analysis. To illustrate the data quality, Figure 2 displays the region of interest of one of the spectra.

The first half of the primary eclipse was observed during the night of 2009 Sep. 11/12. On that night, clouds prevented us from obtaining pre-ingress observations. The second half of the primary eclipse, as well as a num-
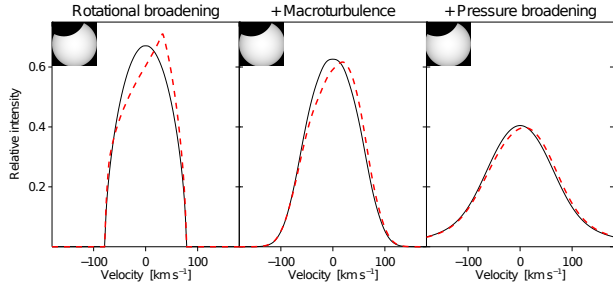
FIG. 4.— **Illustration of the effects of rotation, macro-turbulence, pressure broadening, and eclipse blockage on the absorption line model.** In each panel, the solid line represents an absorption line out of eclipse, while the (red) dashed line shows the same line just before mid-eclipse. The left panel shows only the effect of stellar rotation. The middle panel shows broadening by rotation and macro-turbulence (as appropriate for the Mg II line). The right panel shows a line additionally affected by pressure broadening (as appropriate for the He I line).
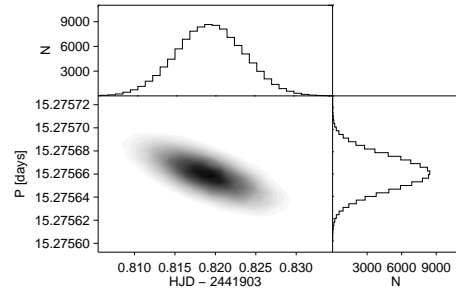

FIG. 5.— **Results for the timing parameters**, based on our Monte Carlo analysis of the times of minimum light given by Ahn (1992). The gray shading indicates the density of Monte Carlo results. The marginalized probability distributions are shown on the sides.

ber of spectra directly after egress, were observed during the night of 2009 Oct. 12/13. Strong wind and poor seeing caused lower SNRs than we had anticipated. In addition, we gathered some spectra on days spread throughout September to November 2009, in order to establish the spectroscopic orbit. All together, 27 spectra were obtained during primary eclipse, 8 spectra were obtained directly after the end of egress, and another 11 observations at various orbital phases outside of eclipses, for a total of 46 spectra. We also attempted photometry of the eclipse throughout autumn and winter of 2009/2010, but all our attempts were foiled by bad weather.

The two-dimensional reduced spectra were examined[2], and bad pixels were flagged and omitted from subsequent analysis. The spectra were shifted in wavelength to account for the radial-velocity of the observatory relative to NY Cep. Initial flat fielding was performed using the nightly blaze functions. We adopted the wavelength solution delivered by the spectrograph software, which has an uncertainty of order 1 m s^{-1} and is negligible for our purposes.

2.1. Description of the model

Our analysis focused on the 11th échelle order of the *Sophie* CCD, which encompasses the wavelength range from 4459 Å to 4486 Å, including the two best absorption lines available for this study, He I (4471 Å) and Mg II (4481 Å). The helium line is strong, with a line width dominated by pressure broadening. The magnesium line is relatively weak but has the virtue of being chiefly broadened by rotation and therefore well-suited to the analysis of the RM effect. There are also a number of other weaker lines in this order that must be modeled simultaneously with the stronger lines. The lines are illustrated in Figure 3, which shows the spectrum of each star individually, after disentangling them with the modeling procedure described in this section. The spectrum from that order was binned to a resolution of about 9 km s^{-1}, giving 213 pixels in the region of interest. The SNR was estimated from the scatter in the continuum on both sides of the He I (4471 Å) and Mg II (4481 Å) lines.

Our spectral model is similar to the models described in Papers I and II. Because of the light from the foreground star, we cannot treat the RM effect as a simple wavelength shift, as is commonly done for eclipses of stars by planets. Instead we modeled the line profiles of both stars simultaneously, taking into account stellar rotation, surface velocity fields, orbital motion, and partial blockage during eclipses. By adjusting the parameters of the model to fit the observed spectra, we derived estimates of the orbital and stellar parameters.

For each star, and for each phase of the eclipse, we created a discretized stellar disk with about 200,000 pixels in a cartesian coordinate system. We assumed the disk to be circular, since the stars are well detached and have slow rotation speeds relative to the breakup velocity. Each pixel has its own emergent spectrum, weighted in intensity according to a linear limb-darkening law, and Doppler shifted due the combined effects of orbital motion, rotation, and macroturbulence. The orbital motion is specified by a Keplerian model common to all pixels. The rotation is assumed to be uniform (no differential rotation). Following Gray (2005), the macroturbulent velocity field is assumed to obey Gaussian distributions for the tangential and radial components, with equal amplitudes, brightnesses, and surface fractions.

The sky-plane coordinates of the foreground and background stars are calculated, and if the background star is being eclipsed then the eclipsed pixels are assigned zero intensity. The emergent spectra from the uncovered pixels of both stars are summed to create a model absorption line kernel. For the He I line a further convolution with a Lorentzian function is applied, to account for pressure broadening. Figure 4 illustrates the effects of rotation, macroturbulence, pressure broadening, and eclipse blockage on the model absorption line kernel.

The kernel is then convolved with a line-list in the wavelength region between 4460 Å and 4485 Å. The positions and line strengths are obtained from the Vienna Atomic Line Database (VALD)[3] for the stellar parameters given by Holmgren et al. (1990) and are listed in Table 2. The He I, Mg II, Al III and some of the O II lines consist of multiple lines with energy levels spaced closely enough (≤ 0.3 Å) that we model them as single lines. We also omitted one S III line which has nearly the same wavelength as one of the O II lines.
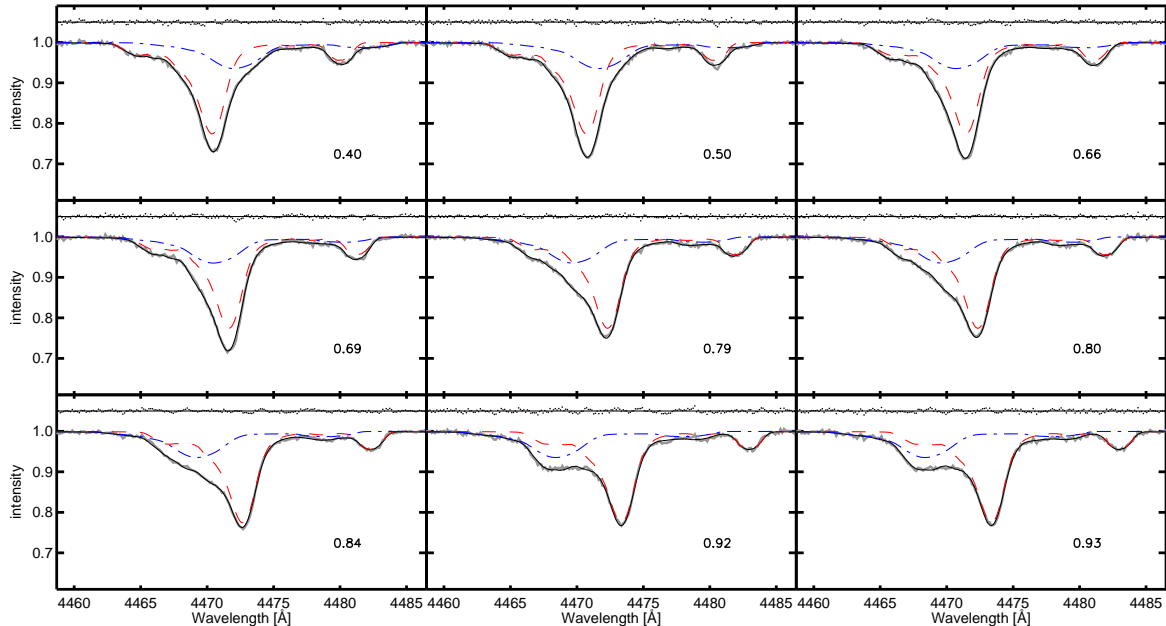
Fig. 6.— **Observations of NY Cep outside of eclipses.** These panels show spectra of both stars in the NY Cep system in the spectral region around the He I line at 4471 Å and Mg II line at 4481 Å. The number in each panel indicates NY Cep's orbital phase at time of observation, defined such that phase 0 corresponds to periastron. The gray solid lines represent the data and the (red) dashed and (blue) dash-dotted lines are the simulated absorption lines of the primary and secondary, respectively. The black line is the best fitting model. The dots around the line at a flux level of 1.05 represent the differences between the data and the model.

2.2. *Eclipse timing*

Since we did not obtain new photometric data, we relied on the data presented by Ahn (1992) (in their Table 2) to constrain the orbital period and time of primary minimum light. The lack of error estimates by Ahn (1992) presented a complication, which we dealt with as follows. We fitted a linear function of epoch to the reported times, assuming equal errors in all the measurements, determined by the requirement $\chi^2 = N_{\rm dof}$. The resulting error in each time was 0.012 days, and the resulting ephemeris are given in Table 3. Our result for the period agrees with that given by Ahn (1992), although we found a slightly different time of primary minimum light, presumably due to different weighting of the measurements.

TABLE 3
Results eclipse timings

Parameter	This work	Ahn (1992)
Period	$15^{\rm d}\!.27566 \pm 0.00002$	$15^{\rm d}\!.27566$
$T_{\rm min,I}$ 1973 [HJD-2 400 000]	41903.819 ± 0.006	41903.8161
$T_{\rm min,I}$ 2009 [HJD-2 400 000]	55117.265 ± 0.016	

Then we used a Monte Carlo approach to calculate the predicted times of minimum light at the epochs of our observations, in a manner that respects the correlation between the parameters of the ephemeris. We created 10^5 fake data sets by adding Gaussian perturbations to the times of minima of Ahn (1992), with a standard deviation of 0.012 days. We then fitted a line to each of

these fake data sets and used the linear fit to calculate the expected mideclipse time on 2009 Oct. 12/13, the last night of our eclipse observations. The mean and standard deviation among all 10^5 results were taken to be the value and the error in the mideclipse time. The results are given in Table 3.

2.3. *The fitting procedure*

We now describe the model parameters in detail. Seven parameters describe the Keplerian orbit: the time of minimum light ($T_{\rm min,I}$), the eccentricity (e), the argument of periastron (ω), the velocity semiamplitudes of the primary and secondary ($K_{\rm p}$ and $K_{\rm s}$), and the velocity offsets ($\gamma_{\rm p}$ and $\gamma_{\rm s}$).[4] We held the period (P) fixed, as its uncertainty is negligible over the 3 months spanned by our observations.

Another 4 free parameters specify the photometric aspects of the eclipse: the light ratio between the two stars at the wavelength of interest ($L_{\rm s}/L_{\rm p}$ at 4500 Å), the fractional radii of the stars ($r_{\rm p}$ and $r_{\rm s}$), and the orbital inclination (i_o). The linear limb darkening parameter ($u_{\rm i}$) was held fixed at 0.4 for both stars (Gray 2005).

The model of the velocity fields introduces 6 parameters: the projected equatorial rotation speeds ($v \sin i_{\rm p}$

---

[4] The velocity offsets are approximately equal to the radial velocity of the NY Cep barycenter with respect to the Solar system barycenter, but the offsets can differ from each other due to subtle factors specific to each star, such as the gravitational redshift and line blending. The latter term refers to the fact that the stars have slightly different strengths and positions of closely spaced lines (unresolved in our spectra), due to the differences in effective temperature, surface gravity, and other atmospheric parameters. These differences can result in a systematic bias in the inferred systemic velocity.
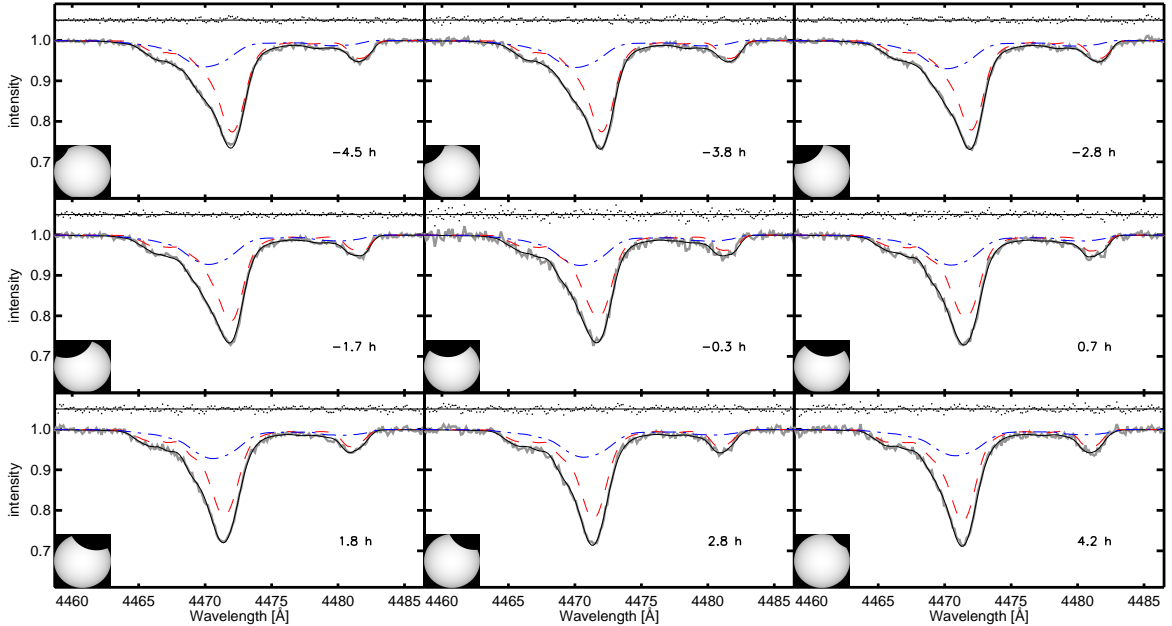
Fig. 7.— **Observations of NY Cep during primary eclipse.** Similar to Figure 6, but for spectra obtained during primary eclipse. The number in each panel indicates the time from mideclipse, in hours. The corner of each panel shows an illustration of the eclipse phase. In the best-fitting model, $\beta_{\rm p} = 2 \pm 4°$, indicating a close spin-orbit alignment. Focusing on the Mg II line, one can see in particular for the observations at -2.8 h and 2.8 h how the RM-effect creates a redshift during the first half of the eclipse and a blue shift during the second half of the eclipse. For the observation at -0.3 h, near mideclipse, blue and redshifted light are blocked by similar amounts.

and $v\sin i_{\rm s}$), the Gaussian width of the macroturbulence for the primary star ($\zeta_{RT}P$), the half-width at half-maximum of the Lorentizan function representing pressure broadening for each star ($\xi_{\rm p}$ and $\xi_{\rm s}$), and finally, the parameters of greatest interest for this study, the sky-projected spin-orbit angle ($\beta_{\rm p}$). The angle is defined according to the convention of Hosokawa (1953), such that $\beta = 0°$ when the axes are parallel, $\beta = \pm 90°$ when they are perpendicular, and $\beta > 0$ when the time-integrated RM effect is a redshift for an orbit with $i_o < 90°$.[5] The macroturbulence parameter for the secondary was held fixed to $20\,{\rm km\,s^{-1}}$, since the secondary is significantly fainter than the primary, causing the results to be insensitive to this parameter.[6]

Eight additional parameters are needed for each star to describe the relative depth of the spectral lines in the wavelength range being modeled. In addition, 3 free parameters are needed to describe the quadratic function used to normalize the continuum level of each of the 46 spectra. The total number of parameters is therefore 7 (orbital) + 4 (photometric) + 6 (velocity fields) + 8×2 (line depths) + 3×46 (normalization), for a total of 171 adjustable parameters. Although this may seem like a large number, the 138 normalization parameters are "trivial" in the sense that they can be opti-

mized separately in subsets of 3, for a given choice of the other parameters. Also, several of the other parameters are subject to *a priori* constraints. More detail on these points is given below.

The fitting statistic was

$$\chi^2 = \sum_{i=1}^{46} \sum_{j=1}^{213} \left[\frac{f_{\lambda_{i,j}}({\rm obs}) - f_{\lambda_{i,j}}({\rm calc})}{\sigma_i} \right]^2 +$$
$$\left(\frac{{\rm T_{minI}} - 2455117.265}{0.016} \right)^2 +$$
$$\left(\frac{i_o - 78°}{1°} \right)^2 + \left(\frac{{\rm L_s/L_p} - 0.37}{0.06} \right)^2 +$$
$$\left(\frac{R_{\rm p}/R_\odot - 6.8}{0.7} \right)^2 + \left(\frac{R_{\rm s}/R_\odot - 5.4}{0.5} \right)^2,$$

where $f_{\lambda_{i,j}}({\rm obs})$ is the observed flux in pixel j in observation i and $f_{\lambda_{i,j}}({\rm calc})$ is the calculated flux based on a particular choice of the model parameters, and σ_i represents the uncertainty in the flux pixel for observation i. The latter was taken to be the reciprocal of the SNR, estimated as described in section 2. In this equation, the first two terms represent the usual sum-of-squares, and the remaining terms represent Gaussian priors based on the results of Holmgren et al. (1990) (except for $T_{\rm min,I}$, which was discussed in the previous section).

To optimize the parameters we used Levenberg-Marquardt (LM) least-squares minimization. The main optimization was conducted for the nontrivial parameters. However, whenever χ^2 was computed within that process, the values of the trivial (normalization) param-

---

[5] The parameter λ, which was introduced by Ohta et al. (2005) and is commonly used in the exoplanet community, is simply $-\beta$.

[6] Indeed, although we included macroturbulence for completeness, the key results for $\beta_{\rm p}$ do not depend on the details, and similar results were obtained even when macroturbulence was ignored. One can see from Figure 4 that macroturbulence has only a small effect on the overall shape of the model absorption line, given the high $v\sin i$ of the primary. This is even more true of the secondary, which rotates about twice as fast as the primary.
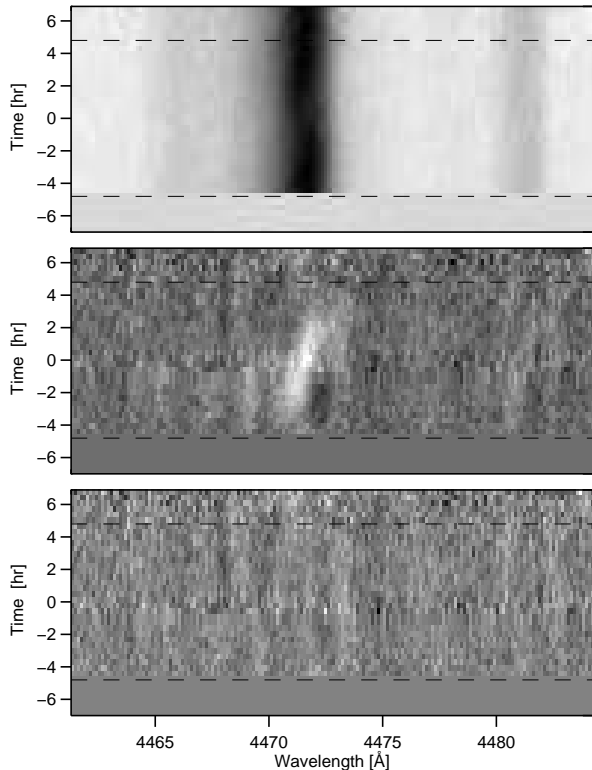
FIG. 8.— **Observations of NY Cep during primary eclipse.** *Top.*—Grayscale depiction of the spectra obtained during and after primary eclipse. Each spectrum is shifted into the rest frame of the primary star, and the best-fitting model of the secondary spectrum has been subtracted. The most prominent lines are He I (seen here blended with the weaker O II lines) and Mg II 4481 Å . Dashed lines indicate the beginning and end of the eclipse. *Middle.* —The same as the top panel, after subtracting the mean absorption line profile shown in Figure 3. The RM effect is evident as the white residual traveling from the blue to the red as the eclipse progresses. *Bottom.*— Residuals between best fitting model and data.

FIG. 9.— **Apparent radial velocities of NY Cep. a:** The apparent radial velocity (RV) of the primary (red filled circles) and secondary (blue open circles) as a function of orbital phase. The line positions were determined by fitting Gaussian functions. The solid line is the calculated radial velocity based on our model to the shape ob the absorption lines, including Keplerian motion and the RM effect. **b,c:** Close-ups of the RM effect during the primary eclipse. The upper panel shows the RM effect plus orbital motion and the lower panel shows only the RM effect, a redshift during the first half of the eclipse, and a blueshift during the second half. One can see that a fit to the RV data would overestimate the amplitude of RM signal. We emphasize that the eclipse radial velocities are shown here for illustration only, as a concise visual summary of the complex distortions of the eclipse spectra: they were not used in our quantitative calculations.

eters were first optimized using a separate 3-parameter minimization for each order. This process is equivalent to the "Hyperplane Least Squares" method that was described and tested by Bakos et al. (2010). To estimate the parameter uncertainties, we used the bootstrap method described by Press et al. (1992), with 5×10^3 realizations.

With 171 parameters, 5 Gaussian priors, and 46×213 data pixels, there are 9632 effective degrees of freedom. The best-fitting model has $\chi^2 = 9148$, or $\overline{\chi}^2 = 0.95$. The low $\overline{\chi}^2$ is probably the result of underestimating the SNR of the relevant lines. The estimate was based on the continuum nearer to the edges of the order, where the SNR is lower (see Figure 2). We have not attempted to correct for this effect.

3. RESULTS

The results for the model parameters are given in Table 4. Figure 6 shows the model fitted to a few out-of-eclipse spectra in the vicinity of the He I and Mg II lines. Figure 7 shows the same for a few of the spectra obtained during primary eclipse. A grayscale representation of the eclipse spectra and post-egress spectra is shown in figure 8. We also display the apparent radial
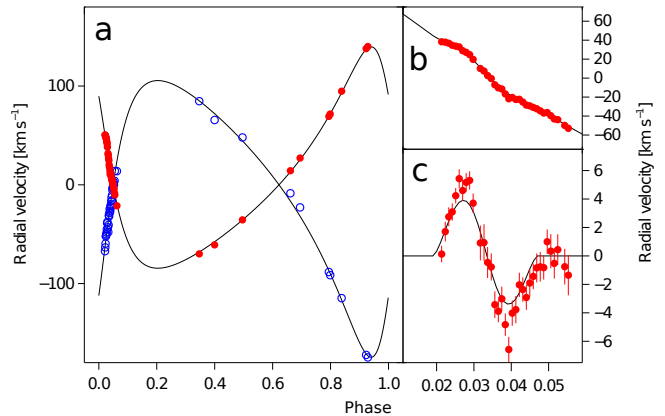
velocities in NY Cep in figure 9.

3.1. Orbital parameters

Our result for T_{minI} is 1.2σ away from the value calculated from the older eclipse timings. Since the ephemeris is based on observations obtained more than 20 years ago, and we do not know the true uncertainty in each measurement, we regard this as good agreement. Likewise the eccentricity is within 2σ of the value given by Holmgren et al. (1990). The measured value for ω agrees with the previous value, but as it is expected to change over time due to apsidal motion a more careful comparison is needed, as discussed in section 4.

Our results for K_p and γ_p agree with the values found by Holmgren et al. (1990). However, our results for the secondary star are different: we find a lower value for K_s, and we found $\Delta\gamma \equiv \gamma_\text{s} - \gamma_\text{p}$ to be consistent with zero. In contrast, Holmgren et al. (1990) found the secondary to be redshifted by $26 \, \text{km s}^{-1}$ relative to the primary, and Heard & Fernie (1968) found an even greater difference of $32 \, \text{km s}^{-1}$. We speculate that the previous measurements were subject to bias because of the relative faintness of the secondary, its rapid rotation, and the need to use pressure-broadened (and asymmetric) lines. Based on the agreement in γ_p it seems that the systemic velocity has not changed significantly over the last decades.

3.2. Stellar parameters

We further find with our fit to all spectra a luminosity ratio $(\text{L}_\text{s}/\text{L}_\text{p})$ of 0.36 ± 0.05 at 4500Å. This result agrees with the value 0.35 that is obtained from comparing the equivalent widths of the He I (4471 Å) line profiles shown

TABLE 4
PARAMETERS OF THE NY CEPHEI SYSTEM.

Parameter	This work	Literature values
Orbital parameters		
Time of primary minimum, $T_{min,I}$ [HJD$-2\,400\,000$]	55117.287 ± 0.009	$41903.8161^{\dagger}$
Period, P [days]	15.27566 (fixed)	$15.27566^{\dagger}$
Eccentricity, e	0.443 ± 0.005	$0.48\pm0.02^{\star}$
Argument of periastron, ω [deg]	56.3 ± 1	$58\pm2^{\star}$
Orbital inclination, i_o [deg]	78.8 ± 0.7	$78\pm1^{\star}$
Velocity semiamplitude (primary), K_p [km s^{-1}]	113.8 ± 1.2	$112\pm2^{\star}$
Velocity semiamplitude (secondary), K_s [km s^{-1}]	139 ± 4	$158\pm8^{\star}$
Velocity offset (primary), γ_p [km s^{-1}]	-17.3 ± 0.7	$-15\pm2^{\star}$
Velocity offset (secondary), γ_s [km s^{-1}]	-21 ± 4	$9\pm6^{\star}$
Stellar parameters		
Light ratio, L_s/L_p	0.36 ± 0.05	$0.37\pm0.06^{\star}$
Fractional radius (primary), r_p	0.086 ± 0.007	
Fractional radius (secondary), r_s	0.084 ± 0.009	
Projected rotation speed (primary), $v\sin i_p$ [km s^{-1}]	78 ± 3	$75\pm10^{\star}$
Projected rotation speed (secondary), $v\sin i_s$ [km s^{-1}]	155 ± 6	$125\pm14^{\star}$
Macroturbulence parameter (primary), ζ_p [km s^{-1}]	23 ± 6	
Macroturbulence parameter (secondary), ζ_s [km s^{-1}]	20 (fixed)	
Pressure broadening parameter (primary), ξ_p [km s^{-1}]	36 ± 1	
Pressure broadening parameter (secondary), ξ_s [km s^{-1}]	54 ± 6	
Linear limb darkening parameter (primary), u_p	0.4 (fixed)	
Linear limb darkening parameter (secondary), u_s	0.4 (fixed)	
Projected spin-orbit angle (primary), β_p [°]	2 ± 4	
Indirectly derived parameters		
Projected orbital semimajor axis, $a\sin i$ [$R_\odot$]	68.6 ± 1	$71.4\pm2.2^{\star}$
$M_p\sin^3 i$ [$M_\odot$]	$10.1^{+0.8}_{-0.6}$	$12\pm1^{\star}$
$M_s\sin^3 i$ [$M_\odot$]	$8.3^{+0.5}_{-0.3}$	$8.7\pm0.6^{\star}$
Primary mass, M_p [$M_\odot$]	$10.7^{+0.9}_{-0.7}$	$13\pm1^{\star}$
Secondary mass, M_s [$M_\odot$]	$8.8^{+0.6}_{-0.4}$	$9\pm1^{\star}$
Primary radius, R_p [$R_\odot$]	6.0 ± 0.5	$6.8\pm0.7^{\star}$
Secondary radius, R_s [$R_\odot$]	5.8 ± 0.5	$5.4\pm0.5^{\star}$

† Data from Ahn (1992)

⋆ Data from Holmgren et al. (1990)

in Figure 3.[7] Both values are consistent with 0.37 ± 0.06 found by Holmgren et al. (1990), based on spectrophotometry.

Our model gives projected rotation speeds of 78 ± 1 km s^{-1} for the primary 155 ± 4 km s^{-1} for the secondary. The width of the Gaussian function describing the macroturbulence in the primary is 23 ± 3 km s^{-1}, and the half-width at half-maximum of the Lorentzians describing pressure broadening are 36 ± 1 km s^{-1} and 54 ± 6 km s^{-1}. These error estimates must be understood as internal to our model, which we recognize may not be completely realistic, especially as it pertains to pressure broadening. We have assumed that absorption lines form at a specific value of pressure, which is not necessarily true. For this reason, the Lorentzian widths have no simple physical interpretation, and the results may be somewhat biased for all other parameters affecting line broadening (namely $v\sin i$ and ζ). For comparisons to

other analyses obtained with different instruments and different analysis procedures, we recommend using the more conservative error estimates given in Table 4. For the projected rotation rates, we find a similar result for the primary as did Holmgren et al. (1990), but we find a significantly higher $v\sin i$ for the secondary, perhaps for the same reasons given in section 3.1.

As for the projected spin-orbit angle β_p, the focus of this study, we find $\beta_p = 2\pm4°$. There is no correlation between this parameter and the linewidth parameters, so the concerns raised above about the oversimplified pressure-broadening model do not apply here. A strong correlation does exist with the time of minimum light (see Figure 10). This implies that future photometric observations to refine the eclipse ephemeris would lead to smaller uncertainty in β_p, although the uncertainty is already quite small.

The absolute radii of the stars can be calculated from the fractional radii and the other orbital parameters. We find radii consistent with the values given in the literature, $R_p = 6.0\pm0.5\,R_\odot$ and $R_s = 5.8\pm0.6\,R_\odot$, which is not surprising since our results were strongly influenced

[7] In estimating the luminosity ratio from the EWs, we accounted for the small increase ($\sim10\%$) in the EW of this line towards lower temperatures in the spectral range from to B0 to B2. See Figure 1 of Leone & Lanzafame (1998).
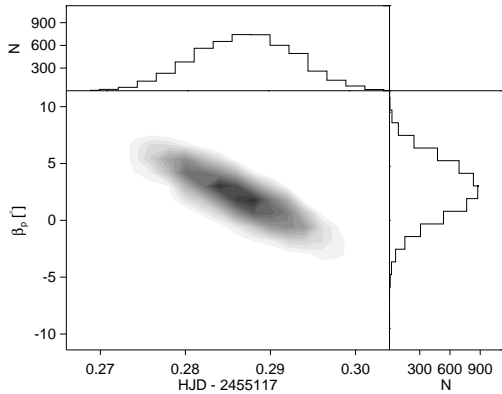
FIG. 10.— **Results for time of minimum light and $\beta_{\mathbf{p}}$**, based on our analysis of the stellar spectra using the bootstrap method. There is a strong correlation between these two parameters.

by the priors on those parameters. For the stellar masses, we find $M_{\mathrm{p}} = 10.7 \pm 0.8\,M_{\odot}$ and $M_{\mathrm{s}} = 8.8 \pm 0.5\,M_{\odot}$ for the primary and secondary, respectively. The value found for the primary is smaller than that reported previously, due to the previously mentioned discrepancy in the velocity semiamplitude of the secondary.

4. DISCUSSION

Primary spin axis— We have measured the angle between the projections of the orbital and stellar angular momentum vectors for the primary star in NY Cep and find that these projections are aligned within the uncertainty of our measurement ($\beta_{\mathrm{p}} = 2 \pm 4°$). We believe this result to be robust, even if our model is simplified in many respects. We have neglected any changes in the limb-darkening law within the lines as compared to the continuum, as well as a number of other "second-order" effects, such as gravity brightening and differential rotation. We experimented with more complex models including these phenomena and found that they produced effects too small to affect our conclusions about spin-orbit alignment. Likewise we experimented with a "two-layer" model for the pressure-broadened lines [see figure 11.5 of Gray (2005)] and found that while it provided a slightly better fit to the data, it introduced several new free parameters and led to no significant changes in any other parameters.

Our result for β_{p} gives a lower bound on the true angle between the stellar and orbital spins, the obliquity (ψ). We however expect the obliquity to be not much larger than β unless the primary spin axis is highly inclined towards the line of sight, an unlikely scenario.

Absolute dimensions— For our discussion we adopt the effective temperatures derived by Holmgren et al. (1990), which are printed in table 2. Because we do not have any new photometry, we do not attempt to derive new effective temperatures or a new age for the system. We adopt the previous classification of NY Cep as a young system ($\sim$6 Myr) at a distance of $750 \pm 90\,\mathrm{pc}$, making it consistent with membership in the Cepheus OB III association. Our finding of a lower mass for the primary does not change the picture of NY Cep significantly given the uncertainties in other parameters.

Stellar rotation— If the spin periods were equal to the orbital period, then the stellar rotation velocities would be 20 km s^{-1} and 19 km s^{-1}, for the primary and secondary, respectively. These numbers are smaller than our results for $v \sin i$, which are 78 ± 3 km s^{-1} and 154 ± 6 km s^{-1}. Assuming $\psi = 0$ for both stars, the implied rotation periods are 3.9 and 1.9 days.

The stars do not seem to be pseudosynchronized, either. The ratio of rotational to orbital frequencies is 3.9 and 8.0 for the primary and secondary, respectively. In the Hut (1981) model of pseudosynchronization, the ratio would be 2.3, which is lower than the observed ratios. If the stars had been significantly influenced by tidal evolution, then one would expect the rotational frequency to be smaller for the secondary star than for the primary star, because the less massive star should synchronize first. In contradiction with this expectation, we observe the secondary to have a higher rotation frequency than the primary.

All of these findings are in agreement with a picture in which the system is only a few million years old, and tidal forces have not had enough time to alter the rotational state of the stars after their arrival on the zero-age main sequence.

Apsidal motion— With the data at hand it is not possible to investigate the internal structures of the two stars in a stringent way via observations of apsidal motion. Firstly, the uncertainties in the radii and ages are so high that the theoretical expected apsidal motion has a high uncertainty. Using the system parameters, together with internal structure constants of $k_2 = -0.080 \pm 0.35$[8] for both stars, we derive an expected apsidal motion rate of 19^{+41}_{-9} arcsec per cycle. Secondly, the measurements of the argument of the periastron (ω) are also quite uncertain. Using the values from Heard & Fernie (1968), who derived an ω of 50.9 ± 3.7, from Holmgren et al. (1990), and from this work, we derive a measured apsidal motion rate of 6 ± 11 arcsec per cycle. Therefore the expected and measured apsidal motions are consistent, but the bounds are too weak to give additional information. To make progress on this field both the expected and measured values for the apsidal motion have to have greater precision and accuracy.

5. CONCLUSION

Through an analysis of high resolution spectra of the NY Cep system, observed during and outside of primary eclipse, we have calculated the orbital and primary and secondary parameters. We also reanalyzed times of minima from the literature to obtain an updated ephemeris for the epoch of our spectroscopic observations. We find a $\sim$15% smaller mass for the primary star than earlier studies, and derive results for the other parameters that are similar to those reported in the literature values.

We measured the angle on the sky between the primary spin axis and the orbital axis by exploiting the Rossiter-McLaughlin (RM) effect. We find that the projections of these axes on the sky are closely aligned ($\beta_{\mathrm{p}} = 2 \pm 4$). The close alignment does not seem to have been the result of tidal evolution, because tidal evolution would also have

---

[8] We estimated the apsidal motion constants using tables from Claret (1995).

synchronized the rotational and orbital periods, which is not observed.

The finding of a close spin-orbit alignment is in strong contrast to the situation in the other young, early type, detached close binary, DI Her, for which the orientation of the axes has been measured (Paper II). For that system we found strongly misaligned spin and orbital axes. While NY Cep and DI Her are similar in that they both harbor young, well detached, early type stars, and have high orbital eccentricities their formation and/or evolution seem to have taken quiet different routes.

DI Her and NY Cep are currently the only early-type detached binaries for which the orientation of the stellar spin axes is known. Both systems are on eccentric orbits, have detached components, and are young enough to exclude any development of the spin-orbit alignment during main-sequence life due to tidal interactions. Yet the axes in the DI Her system are strongly misaligned ($\beta_\mathrm{p} = 72 \pm 4$; $\beta_\mathrm{s} = -84 \pm 8$) while the primary axis in NY Cep is well aligned ($\beta_\mathrm{p} = 2\pm4$). Indeed, the projected alignment of NY Cep is even closer than the alignment between the Sun's spin axis and the ecliptic plane ($7°$).

As of yet there is no good explanation for the misalignment of DI Her. Broadly speaking, it could be primordial, or it could be the result of an interaction between the stars or between the stars and the disk from which they formed, or it could be due to torques from additional bodies in the system. The results in this paper do not point to a particular mechanism, but they do mean that any successful theory must pass the "NY Cep" test, namely, it must explain the difference between those two systems.

Obtaining measurements of spin orbit angles in a number of early type close binary systems might reveal which environmental variables determine the orientation of stellar rotation axes in these systems. For example if the interaction with a distant companion via the Kozai migration (Fabrycky & Tremaine 2007) formed close binaries, than misaligned systems should be more likely to have a detected companion and closer systems might be more likely to have misaligned axes than wider systems. If alignment is a simple function of coherence length during star formation, then the opposite should be true: the closer the system, the stronger the tendency toward alignment.

This is why we have started a small survey to measure the orientation of stellar spin axes in other early-type binaries.

REFERENCES

Abt, H. A. 2001, AJ, 122, 2008
Ahn, Y. S. 1992, Ap&SS, 198, 137
Albrecht, S., Reffert, S., Snellen, I., Quirrenbach, A., & Mitchell, D. S. 2007, A&A, 474, 565
Albrecht, S., Reffert, S., Snellen, I. A. G., & Winn, J. N. 2009, Nature, 461, 373
Andersen, J., Nordstrom, B., Garcia, J. M., & Giménez, A. 1987, A&A, 174, 107
Bakış, V., Budding, E., Erdem, A., Bakış, H., Demircan, O., & Hadrava, P. 2006, MNRAS, 370, 1935
Bakos, G. Á., et al. 2010, ApJ, 710, 1724
Bate, M. R., Lodato, G., & Pringle, J. E. 2010, MNRAS, 401, 1505
Bonnell, I., Arcoragi, J., Martel, H., & Bastien, P. 1992, ApJ, 400, 579
Chelli, A., & Petrov, R. G. 1995, A&AS, 109, 401
Claret, A. 1995, VizieR Online Data Catalog, 410, 90441
Corcoran, M. F., Siah, M. J., & Guinan, E. F. 1991, AJ, 101, 1828
Donar, A., Jensen, E. L. N., & Mathieu, R. D. 1999, in Bulletin of the American Astronomical Society, Vol. 31, Bulletin of the American Astronomical Society, 1490–+
ESA. 1997, ESA SP-1200
Fabrycky, D., & Tremaine, S. 2007, ApJ, 669, 1298
Gaudi, B. S., & Winn, J. N. 2007, ApJ, 655, 550
Giménez, A. 2006, ApJ, 650, 408
Glebocki, R., & Stawikowski, A. 1997, A&A, 328, 579
Gray, D. F. 2005, The Observation and Analysis of Stellar Photospheres, 3rd Ed. (ISBN 0521851866, Cambridge University Press)
Guthrie, B. N. G. 1985, MNRAS, 215, 545
Hadrava, P. 2009, arXiv:0909.0172
Hale, A. 1994, AJ, 107, 306
Harmanec, P. 2002, Astronomische Nachrichten, 323, 87
Heard, J. F., & Fernie, J. D. 1968, JRASC, 62, 99
Hébrard, G., et al. 2008, A&A, 488, 763

Hirano, T., Suto, Y., Taruya, A., Narita, N., Sato, B., Johnson, J. A., & Winn, J. N. 2010, ApJ, 709, 458
Holmgren, D. E., Scarfe, C. D., Hill, G., & Fisher, W. 1990, A&A, 231, 89
Holt, J. R. 1893, A&A, 12, 646
Hosokawa, Y. 1953, PASJ, 5, 88
Howe, K. S., & Clarke, C. J. 2009, MNRAS, 392, 448
Hube, D. P., & Couch, J. S. 1982, Ap&SS, 81, 357
Hut, P. 1981, A&A, 99, 126
Jensen, E. L. N., Mathieu, R. D., Donar, A. X., & Dullighan, A. 2004, ApJ, 600, 789
Kopal, Z. 1959, Close binary systems (The International Astrophysics Series, London: Chapman & Hall, 1959)
Kozai, Y. 1962, AJ, 67, 591
Lai, D., Foucart, F., & Lin, D. N. C. 2010, ArXiv e-prints
Lázaro, C., Arévalo, M. J., & Antonopoulou, E. 2006, MNRAS, 368, 959
Lázaro, C., Martínez-Pais, I. G., & Arévalo, M. J. 2004, MNRAS, 351, 707
Le Bouquin, J., Absil, O., Benisty, M., Massi, F., Mérand, A., & Stefl, S. 2009, A&A, 498, L41
Leone, F., & Lanzafame, A. C. 1998, A&A, 330, 306
McLaughlin, D. B. 1924, ApJ, 60, 22
Monin, J., Menard, F., & Duchene, G. 1998, A&A, 339, 113
Monin, J., Ménard, F., & Peretto, N. 2006, A&A, 446, 201
Narita, N., Sato, B., Hirano, T., & Tamura, M. 2009, PASJ, 61, L35
Ohta, Y., Taruya, A., & Suto, Y. 2005, ApJ, 622, 1118
Perruchot, S., et al. 2008, in SPIE Conference Series, Vol. 7014
Petrov, R. G. 1989, in NATO ASIC Proc. 274: Diffraction-Limited Imaging with Very Large Telescopes, ed. D. M. Alloin & J.-M. Mariotti, 249
Popper, D. M. 1982, ApJ, 254, 203
Press, W. H., Teukolsky, S. A., Vetterling, W. T., & Flannery, B. P. 1992, Numerical recipes in FORTRAN. The art of scientific computing, 2nd Ed. (Cambridge: University Press)

Ratzka, T., et al. 2009, A&A, 502, 623

Rossiter, R. A. 1924, ApJ, 60, 15

Rucinski, S. M. 2009, MNRAS, 395, 2299

Sato, K. 1974, PASJ, 26, 65

Schlaufman, K. C. 2010, ApJ, 719, 602

Schlesinger, F. 1910, Publications of the Allegheny Observatory of the University of Pittsburgh, 1, 123

Skemer, A. J., Close, L. M., Hinz, P. M., Hoffmann, W. F., Kenworthy, M. A., & Miller, D. L. 2008, ApJ, 676, 1082

Soderblom, D. R. 1985, PASP, 97, 57

Soderhjelm, S. 1980, A&A, 89, 100

Struve, O., & Elvey, C. T. 1931, MNRAS, 91, 663

Tremaine, S. 1991, Icarus, 89, 85

Triaud, A. H. M. J., et al. 2010, ArXiv e-prints

Twigg, L. W. 1979, PhD thesis, Florida Univ., Gainesville.

Weis, E. W. 1974, ApJ, 190, 331

Winn, J. N., Fabrycky, D., Albrecht, S., & Johnson, J. A. 2010, ApJ, 718, L145

Winn, J. N., Johnson, J. A., Albrecht, S., Howard, A. W., Marcy, G. W., Crossfield, I. J., & Holman, M. J. 2009, ApJ, 703, L99

Wolf, S., Stecklum, B., & Henning, T. 2001, in IAU Symposium, Vol. 200, The Formation of Binary Stars, ed. H. Zinnecker & R. Mathieu, 295–+

Worek, T. F. 1985, PhD thesis, Pittsburgh Univ., PA.

—. 1996, PASP, 108, 962

Worek, T. F., Zizka, E. R., King, M. W., & Kiewiet de Jonge, J. H. 1988, PASP, 100, 371